

## TITLE PAGE

**Title:** Immuno-PET of innate immune markers CD11b and IL-1 $\beta$  detect inflammation in murine colitis.

**Authors:** Nicole Dmochowska<sup>1</sup>, William Tieu<sup>2</sup>, Marianne D Keller<sup>1,3</sup>, Hannah R Wardill<sup>1</sup>, Chris Mavrangelos<sup>1</sup>, Melissa A Campaniello<sup>1</sup>, Prab Takhar<sup>2</sup>, Patrick A Hughes<sup>1</sup>

### Affiliations:

1: Centre for Nutrition and Gastrointestinal Diseases, Adelaide Medical School, University of Adelaide & South Australian Health and Medical Research Institute, Adelaide, Australia

2: Molecular Imaging and Therapy Research Unit (MITRU), South Australian Health and Medical Research Institute, Adelaide, Australia

3: Preclinical, Imaging & Research Laboratories (PIRL), South Australian Health and Medical Research Institute, Adelaide, Australia

**Conflicts of Interest:** No authors have any personal or financial conflicts of interest.

### Corresponding author:

Dr. P. A. Hughes

Centre for Nutrition and Gastrointestinal Diseases, Level 7 SAHMRI, Adelaide, South Australia, 5000, AUSTRALIA. Phone: +61881284843.

Email: [patrick.hughes@adelaide.edu.au](mailto:patrick.hughes@adelaide.edu.au)

**First author:**

Nicole Dmochowska

Centre for Nutrition and Gastrointestinal Diseases, Level 7 SAHMRI, Adelaide, South Australia, 5000, AUSTRALIA. Phone: +61881284839  
Email: nicole.dmochowska@adelaide.edu.au

Nicole Dmochowska is a current PhD student.

**Word count:** 4990

**Funding support:** This study was funded by a project development grant, University of Adelaide with <sup>89</sup>Zr radiochemistry supported by Bellberry Limited and Bellberry Molecular Imaging Program. Further support was provided by an Australian Government RTP and a William T Southcott Nuclear Medicine Scholarship to ND, a NHMRC C.J. Martin Biomedical Fellowship (#APP1140992) to HRW and a NHMRC R.D. Wright Biomedical Research Fellowship (#APP1105028) to PAH.

**Running title:** Innate immuno-PET in colitis

## ABSTRACT

Inflammatory bowel disease (IBD) is a chronic relapsing and remitting inflammatory disease of the gastrointestinal tract. The diagnosis and monitoring of IBD is reliant on endoscopy which is invasive and does not provide information regarding specific mediators. Symptom flare in IBD is associated with increased activation of innate immune pathways. Immuno-PET approaches have previously demonstrated the ability to detect colitis, however direct comparison of antibodies targeted to innate immune mediators and cells have not been evaluated. We aimed to compare immuno-PET of antibodies to IL-1 $\beta$  and CD11b against standard  $^{18}\text{F}$ -FDG and MRI approaches to detect colonic inflammation. **Methods:** Colonic concentrations of IL-1 $\beta$  and myeloperoxidase (MPO) were determined by ELISA and colonic infiltration by CD11b+ CD3- innate immune cells were determined by flow cytometry and compared between healthy and dextran sodium sulphate treated colitic mice. PET of  $^{89}\text{Zr}$ -labelled  $\alpha$ -IL-1 $\beta$  and  $\alpha$ -CD11b, and  $^{18}\text{F}$ -FDG were compared by volume of interest and MRI by region of interest analysis. Imaging results were confirmed by *ex vivo* biodistribution analysis. **Results:** Colonic inflammation was associated with impaired colonic epithelial barrier permeability, an increase in colonic IL-1 $\beta$  and MPO concentrations, and increased CD11b+ CD3- innate immune cell infiltration into the colon.  $^{89}\text{Zr}$ - $\alpha$ -IL-1 $\beta$  and  $^{89}\text{Zr}$ - $\alpha$ -CD11b immuno-PET detected colonic inflammation, as did  $^{18}\text{F}$ -FDG, and all PET tracers were more sensitive than MRI. While  $^{18}\text{F}$ -FDG volume of interests correlated with colitis severity and a strong trend was observed with  $^{89}\text{Zr}$ - $\alpha$ -IL-1 $\beta$ , no correlation was observed for  $^{89}\text{Zr}$ - $\alpha$ -CD11b or MRI.  $^{89}\text{Zr}$ - $\alpha$ -IL-1 $\beta$  was distributed mainly to the gastrointestinal tract, while  $^{89}\text{Zr}$ - $\alpha$ -CD11b was distributed in more tissue types.

**Conclusion:** Immuno-PET using antibodies directed to innate immune markers detected colonic inflammation, with  $^{89}\text{Zr}$ - $\alpha$ -IL-1 $\beta$  providing a more tissue specific signal than  $^{89}\text{Zr}$ - $\alpha$ -CD11b. Development of these technologies for human subjects will potentially provide a less invasive approach than endoscopy for diagnosing and monitoring IBD.

**Key words:** Immuno-PET, innate immune system, colitis, inflammatory bowel disease.

## INTRODUCTION

Inflammatory bowel disease (IBD) is a collection of chronic idiopathic inflammatory diseases of the gastrointestinal tract, incorporating Crohn's disease (CD) and ulcerative colitis (UC) (1). IBD impacts substantially on quality of life and, while treatable, significant gaps remain due to incomplete efficacy, tolerance and side-effects leading to variable periods of remission and relapse (2). Patients with IBD require constant surveillance as prognostic indicators of symptom flare remain poor and patients with long-standing disease have an increased risk of developing colon cancer (2,3). The diagnosis and management of IBD is currently heavily reliant on endoscopy which is generally well tolerated but is invasive, restricted to imaging of the superficial mucosal surface, is difficult to reach the all areas of the small intestine, and does not provide immediate information regarding specific mediators or mechanisms. Therefore, new technologies are required for imaging IBD that are less invasive than endoscopy and are able to provide information regarding specific pathological processes in real time.

Clinical studies support the use of positron emission tomography (PET), single photon emission computed tomography (SPECT) and magnetic resonance imaging (MRI) for detecting inflammation in the gastrointestinal tract, satisfying the criteria for reduced invasiveness and real-time information (4,5). However, current clinical PET, SPECT and MRI approaches in IBD are restricted to using radiolabeled autologous leukocytes and 2-deoxy-2-<sup>18</sup>F fluoroglucose (<sup>18</sup>F-FDG ) in PET/SPECT and gadolinium contrast in MRI, none of which provide information regarding specific mediators. This

lack of detail is of increasing importance due to the increase in use of target specific biologics, particularly antibodies, and the emergence of personalized medicine.

Monoclonal antibodies have exquisite selectivity for their target and their applicability to immuno-PET has been appreciated for decades, particularly in the cancer field (6-8). However, the use of immuno-PET in IBD is currently limited to preclinical studies where T cell infiltration into the colon of colitic animals has been demonstrated either directly by imaging the T<sub>HELPER</sub> (T<sub>H</sub>) cell marker CD4 (9), or indirectly by targeting the gut homing integrin  $\alpha_4\beta_7$  (10). In contrast, immuno-PET of immune mediators is yet to be reported, however direct labelling of the neutrophil attracting chemokine CXCL8 (also known as IL-8) (11,12) and antibody directed imaging of TNF- $\alpha$  (13) have shown some efficacy for SPECT in both colitic animals and human IBD.

Activation of the innate immune system is intimately linked to inflammation in IBD, most obviously illustrated by the clinical utility of detection of the neutrophil secreted mediators calprotectin and lactoferrin in stool (3). IL-1 $\beta$  is an inducible cytokine that has a key role in innate immune responses and is predominantly secreted by neutrophils, monocyte/macrophages and dendritic cells, while CD11b is a pan-myeloid innate immune marker predominantly expressed on these same cell types. Here we aimed to compare PET of <sup>89</sup>Zirconium (<sup>89</sup>Zr) conjugated antibodies against IL-1 $\beta$  and CD11b to standard (<sup>18</sup>F-FDG) PET and MRI approaches to detect inflammation in colitic mice.

## **MATERIALS AND METHODS**

All experiments were approved by the Animal Ethics Committee of the South Australian Health and Medical Research Institute (SAHMRI) and The University of Adelaide.

### **Mice**

Male C57BL/6jSah mice aged 10-14 weeks (20-30 g) were bred and group housed in a specific pathogen-free environment at SAHMRI. Animals had *ad libitum* access to food and water. Experiments were conducted with only male mice to eliminate the potential confounding effects of the oestrus cycle. Mice were humanely euthanized via CO<sub>2</sub> inhalation and cervical dislocation to remove tissues.

### **DSS Colitis Model**

Colitis was induced by replacing normal drinking water with 2% (w/v) dextran sodium sulphate (DSS) (molecular mass 40 – 50 kDa, Alfa Aesar, Lancashire, United Kingdom) for 5 days, followed by an additional 3 days of normal drinking water. Mice were assessed daily for signs of acute colitis including body weight and diarrhoea. Healthy mice were age and weight matched. Colon length was measured on excised colons dissected free from surrounding tissue from the tip of the anus to the distal end of the cecum.

### **Ussing Chamber Studies**

Distal colon segments were mounted into 0.1 cm<sup>2</sup> aperture sliders bathed in 5 mL baths with oxygenated glucose-fortified Ringers solution for Ussing chamber analysis (Physiologic instruments, CA, USA) as previously described (14). Briefly, voltage clamped tissues were equilibrated for 20 min before baseline trans-epithelial electrical resistance ( $R_{TE}$ ;  $\Omega \cdot \text{cm}^2$ ) and short circuit current ( $I_{SC}$ ;  $\mu\text{A}/\text{cm}^2$ ) were averaged over 10 min.

### **Myeloperoxidase Activity**

Myeloperoxidase (MPO) activity in the distal colon was determined as previously described (15,16). Briefly, PBS washed tissue segments were homogenized in 0.5% hexadecyl-trimethylammonium bromide (Sigma-Aldrich, NSW, Australia) and reacted with *o*-dianisidine hydrochloride (Sigma-Aldrich). Absorbance at 450 nm was averaged over 5 min. with 30 sec. intervals. MPO activity is expressed as unit/mg of tissue with one unit of MPO activity defined as the amount of MPO required to degrade 1  $\mu\text{mol}$  of peroxide per min. at 25°C.

### **IL-1 $\beta$ ELISA**

Proteins were extracted from the distal colon as previously described (14,15). Briefly, colon segments were homogenized for 5 min. in cell extraction buffer (ThermoFisher Scientific, NSW, Australia) supplemented with protease inhibitor cocktail (Sigma-Aldrich), 1 mM phenyl-methanesulfonyl fluoride (Sigma-Aldrich) and 50  $\mu\text{M}$  ethylenediaminetetraacetic acid at 1 mL per 50 mg of tissue. The lysate was incubated (1 hour, 4°C with rotation), sonicated (2 min.) and centrifuged (14,000 rpm, 15 min.,

4°C). Supernatant was collected and stored at -80°C until analysis. IL-1 $\beta$  concentrations were determined by OptEIA IL-1 $\beta$  ELISA set (BD Biosciences, NSW, Australia) as previously described (14,15). The limit of sensitivity was <4 pg/mL. Concentrations were normalized to total protein concentration as determined by a BCA assay (Abcam, UK) as previously described (15).

### **Flow Cytometry**

Colon lamina propria mononuclear cells (LPMCs) were isolated enzymatically essentially as previously described (14,15). Briefly, the colon was excised free of fat and blood vessels, flushed with cold PBS roughly chopped and incubated in HEPES buffered HBSS supplemented with 1mM ethylenediaminetetraacetic and 1mM dithiothreitol (20 min., 37°C, gentle shaking). Tissue segments were filtered (100  $\mu$ M) and remaining tissue minced and incubated in complete RPMI 1640 (Gibco, Germany) supplemented with fetal calf serum, glutamax, penicillin/streptomycin, 1 mg/mL Collagenase D, 0.5 mg/mL DNase1 and 3 mg/mL Dispase (all from Sigma-Aldrich) (20 min. 37°C, gentle shaking) before straining (40  $\mu$ M) and , resuspending over a 40/80 percoll gradient and the interphase LPMC layer collected and pelleted for LPMC. Viability was determined (trypan blue) and only preparations with  $\geq$  80% viability were investigated further.  $0.5 \times 10^6$  Fc blocked LPMC were stained with the anti-mouse monoclonal antibodies CD45-BV605 (30-F11), CD3-BUV395 (145-2C11), CD11b-APC-Cy7 (M1/70) (all from BD Biosciences). 20,000 events per test were analyzed using a FACS-Fortessa (BD Biosciences) and proportions of live (FVS700, BD Biosciences) singlets were determined using FlowJo (Tree Star, OR, USA), as described previously (14,15).

## **Antibody-chelator Conjugation and Radiolabeling**

$^{89}\text{Zr}$  oxalate was produced via proton irradiation of  $^{89}\text{Y}$  target on PETtrace 880 cyclotron (GE Healthcare) and purified on Aleco (Comecer, Italy) as previously described (17). Monoclonal  $\alpha$ -CD11b (M1/70) and  $\alpha$ -IL-1 $\beta$  (B122) (BD Biosciences, NSW, Australia) were conjugated to  $^{89}\text{Zr}$  with NCS-Bz-DFO (Macrocyclics, Texas, USA) linkage as previously described (18,19). Competitive blocking assays determined the specificity of  $^{89}\text{Zr}$  conjugated antibodies, whereby  $0.5 \times 10^6$  healthy mouse splenocytes were incubated with  $1.25 \mu\text{g}$  of  $^{89}\text{Zr}$  labelled  $\alpha$ -IL-1 $\beta$  or  $\alpha$ -CD11b for 20 minutes at  $37^\circ\text{C}$ , in the presence or absence of  $50 \mu\text{g}$  of unlabeled  $\alpha$ -IL-1 $\beta$  or  $\alpha$ -CD11b added for 20 min prior. Cells were pelleted and counted using a Hidex gamma-counter for accumulation of  $^{89}\text{Zr}$ . All counts were background and decay corrected.  $^{18}\text{F}$ -FDG (phosphate buffer) was produced by MITRU, SAHMRI on a FASTLab synthesizer (GE Healthcare, UK).

## **MRI-PET**

3-5 MBq  $^{89}\text{Zr}$ - $\alpha$ -IL-1 $\beta$  ( $37.5 \mu\text{g}$ ) and  $\alpha$ -CD11b ( $85 \mu\text{g}$ ) in 100-200  $\mu\text{L}$  saline were administered intravenously (tail vein) 24 hours prior to imaging, while 10-15 MBq  $^{18}\text{F}$ -FDG in 100-200  $\mu\text{L}$  saline was administered intravenously 30 min. prior to imaging. Some mice underwent MRI imaging first. Mice were anaesthetized with isoflurane (2%) and a T2-weighted RARE spin echo sequence was acquired with a benchtop MRI system (Bruker Icon 1T; Bruker Physik GmbH, Germany) (TR/TE= 84/4314 ms, 1 NEX, rare factor =8, voxel  $80 \text{ mm} \times 80 \text{ mm}$ , slice thickness 2mm, scan time < 2 min). ITK snap ([www.itksnap.org](http://www.itksnap.org)) was used for consequent segmentation of the scans (20). PET

experiments were carried out over 15 min. using a submillimetric resolution (0.7 mm) Albira PET-SPECT small animal scanner (Bruker Biospin GmbH, Valencia, Spain). Manually drawn volumes of interest in the area of interest were used to analyze average and total radiotracer accumulation using the PMOD imaging suite (PMOD technologies, Switzerland).

### ***Ex vivo* Biodistribution Studies**

Immediately following culling post-imaging, organs of interest were dissected, weighed and counted for  $^{89}\text{Zr}$  accumulation as outlined above in blocking experiments.

### **Statistical Analysis**

Data are expressed as mean $\pm$ SEM in all cases. The significance of results were determined by unpaired *t* test except for weight loss data where a two-way ANOVA with Bonferroni post-hoc was used. The strength and significance of correlations were determined by Pearson's analysis. Differences with  $P < 0.05$  were considered statistically significant.

## **RESULTS**

### **DSS Colitis is Associated with Body Weight Loss, Colon Shortening and Impaired Epithelial Permeability**

Body weight was reduced in the DSS treated group 4 days after starting treatment ( $P < 0.01$ , Fig 1A), and further reduced by ~10% 8 days after starting treatment ( $P < 0.001$ , Fig 1A). By day 8, DSS treated mice also had ~15% shorter colons ( $P < 0.001$ , Fig 1B), a ~35% reduction in epithelial resistance ( $P < 0.01$ , Fig 1Ci) and a ~60% reduction in short-circuit current ( $P < 0.01$ , Fig 1Cii) indicative of colonic inflammation and damage to the epithelial barrier.

### **Colonic Innate Immune Infiltration is Increased in DSS Colitis**

DSS treated mice had an ~7.5-fold increase in colonic MPO activity ( $P < 0.001$ , Fig 2A) and a ~2.5-fold increase in colonic IL-1 $\beta$  concentration ( $P < 0.01$ , Fig 2B) indicating innate immune mediators are increased in colitic mice. The proportion of CD11b colonic LPMC were increased ~6 fold in DSS treated mice ( $P < 0.001$ , Fig 2C), indicative of an infiltration by innate myeloid cells including neutrophils, monocyte/macrophages and dendritic cells.

### **Immuno-PET Detects Colonic Innate Immune Activation in Colitis**

$^{89}\text{Zr}$  was successfully conjugated to  $\alpha$ -IL-1 $\beta$  and  $\alpha$ -CD11b as demonstrated by outcompeting binding in the presence of excess unlabeled antibody ( $^{89}\text{Zr}$ - $\alpha$ -IL-1 $\beta$ : 8135 $\pm$ 1510 counts per min. (cpm) hot vs 3026 $\pm$ 337 cpm cold  $P < 0.05$ ,  $N=3$ ,  $^{89}\text{Zr}$ - $\alpha$ -CD11b 61535 $\pm$ 8355 cpm hot vs 34811 $\pm$ 4081 cpm cold,  $N=3$ ,  $P, 0.05$ ). PET imaging

revealed distal colonic uptake of  $^{89}\text{Zr-}\alpha\text{-IL-1}\beta$  was increased  $\sim 3$  fold ( $P < 0.001$ , Fig 3Ai, supplemental video 1 and 2),  $^{89}\text{Zr-}\alpha\text{-CD11b}$  was increased  $\sim 5$  fold ( $P < 0.05$ , Fig 3Bi, supplemental video 3 and 4) and  $^{18}\text{F-FDG}$  was increased  $\sim 3.5$  fold ( $P < 0.01$ , Fig 3Ci, supplemental video 5 and 6) in DSS colitic mice. A robust positive correlation ( $R^2 = 0.70$ ,  $P < 0.05$ ) was observed between colonic uptake of  $^{18}\text{F-FDG}$  and % body weight loss (Fig 3Cii), with a strong trend toward a similar effect observed for  $^{89}\text{Zr-}\alpha\text{-IL-1}\beta$  ( $R^2 = 0.54$ ,  $p = 0.09$ , Fig 3Aii), but not for  $^{89}\text{Zr-}\alpha\text{-CD11b}$  (Fig 3Bii).

### **Biodistribution of $^{89}\text{Zr-}\alpha\text{-IL-1}\beta$ and $^{89}\text{Zr-}\alpha\text{-CD11b}$**

*Ex vivo* analysis indicated uptake of  $^{89}\text{Zr-}\alpha\text{-IL-1}\beta$  and  $^{89}\text{Zr-}\alpha\text{-CD11b}$  were increased throughout the gastrointestinal tract in DSS treated mice relative to control mice, but also in some extra-gastrointestinal sites. Specifically, uptake of  $^{89}\text{Zr-}\alpha\text{-IL-1}\beta$  was increased  $\sim 3$  fold in the colon ( $P < 0.05$ ),  $\sim 5$ -fold in the cecum ( $P < 0.01$ ),  $\sim 1.5$ -fold in the small intestine ( $P < 0.05$ ) and  $\sim 1.75$ -fold in the stomach ( $P < 0.05$ ), while uptake in the spleen was also increased  $\sim 1.75$ -fold ( $P < 0.05$ ) (Fig 4A). Uptake was similar between DSS treated and control mice in all other tissues investigated. Uptake of  $^{89}\text{Zr-}\alpha\text{-CD11b}$  was more discrete in the gastrointestinal tract with increases only observed in the colon ( $\sim 26$ -fold,  $P < 0.05$ ) and small intestine ( $\sim 20$ -fold,  $P < 0.05$ ) and a trend toward an increase in the cecum ( $\sim 21$ -fold,  $P = 0.083$ ) (Fig 4B). However, increased uptake of  $^{89}\text{Zr-}\alpha\text{-CD11b}$  was observed in more sites outside of the gastrointestinal tract than  $^{89}\text{Zr-}\alpha\text{-IL-1}\beta$ , including  $\sim 6$ -fold in the spleen ( $P < 0.05$ ), but also  $\sim 7$ -fold in the liver ( $P < 0.05$ ) and  $\sim 8$  fold in the bone marrow ( $p < 0.05$ ). Notably, trends toward increased uptake of  $^{89}\text{Zr-}\alpha\text{-CD11b}$  were observed across most other tissues including the cecum, tail, stomach, however

uptake was generally more variable for  $^{89}\text{Zr-}\alpha\text{-CD11b}$  than for  $^{89}\text{Zr-}\alpha\text{-IL-1}\beta$ , limiting the significance of these observations.

### **MRI Detects Colonic Inflammation in Colitic Mice**

MRI analysis of colonic inflammation revealed an ~2-fold increase of the  $T_2$  signal intensity ratio in DSS colitis relative to control ( $P < 0.01$ , Fig 5i, supplemental video 7 and 8), but this analysis did not correlate with % body weight loss (Fig 5ii).

## DISCUSSION

We demonstrate for the first time that immuno-PET directed against innate immune cells and mediators is applicable for detection of colitis. The sensitivity of  $^{89}\text{Zr}$  labelled  $\alpha\text{-IL-1}\beta$  and  $\alpha\text{-CD11b}$  immuno-PET for detecting colonic inflammation was similar to  $^{18}\text{F-FDG}$ , and all PET approaches were more sensitive than MRI. Furthermore, uptake of  $^{89}\text{Zr-}\alpha\text{-IL-1}\beta$  was restricted to the gastrointestinal tract and spleen while  $^{89}\text{Zr-}\alpha\text{-CD11b}$  was distributed over a broader range of tissue types. Our comparison demonstrates the strong potential that immuno-PET of innate immune mediators has for diagnosing and monitoring IBD.

Activation of the innate immune system is a hallmark of inflammation in IBD both in humans and animal models (3,21). DSS is directly toxic to epithelial cells and we confirm that epithelial damage in DSS colitis is associated with increased colonic infiltration of CD11b expressing cells and increased colonic concentrations of innate immune secreted IL-1 $\beta$  (22), both which we were reliably able to detect by PET of  $^{89}\text{Zr}$  conjugated monoclonal antibodies. Previous immuno-PET studies have identified increased infiltration of T cells in DSS colitis, either by directly labelling the T<sub>H</sub> marker CD4 or by labelling the gut homing integrin complex  $\alpha_4\beta_7$ , which is upregulated on T cells in IBD (9,10,23). However, our study is the first to describe the potential radiolabeled antibodies against innate immune markers have for PET in IBD diagnosis and monitoring.

We observed a striking difference in the biodistribution of  $^{89}\text{Zr-}\alpha\text{-IL-1}\beta$  and  $^{89}\text{Zr-}\alpha\text{-CD11b}$ , where  $^{89}\text{Zr-}\alpha\text{-IL-1}\beta$  was restricted to the gastrointestinal tract and spleen while  $^{89}\text{Zr-}\alpha\text{-CD11b}$  was observed in a broad range of tissues. Furthermore,  $^{89}\text{Zr-}\alpha\text{-IL-1}\beta$  also correlated with colitis severity while  $^{89}\text{Zr-}\alpha\text{-CD11b}$  did not. These findings are likely to relate to immunological processes underlying innate immune activation in colitis. Innate immune cells migrate from induction sites in lymphatic tissue through the blood stream into sites of inflammation where they mature and secrete cytokines including IL-1 $\beta$  before clearing from tissue by the lymphatics or dying (24). CD11b is expressed on innate cell subsets that promote inflammation, such as M1 macrophages and most neutrophil subsets, but also on innate immune cells that promote tolerance, wound healing and immune suppression, including M2 macrophages, dendritic cells and CXCL4 expressing neutrophil subsets (25,26). These cells express CD11b at all stages of maturity and therefore imaging CD11b is likely to detect sites of inflammation but also migration between tissues and lymph nodes including the bone marrow and, particularly in mice, the spleen. Furthermore, while CD11b expression is high on myeloid innate immune cells it is also expressed on other immune cells including T and B cell subsets which may contribute toward the signal we observed in our imaging (27). The expression of individual markers on multiple cell types is common, for example CD4 is expressed on macrophages in addition to T<sub>H</sub> cells, and complex flow cytometry using multiple markers is typically required to conclusively characterize individual immune cell subsets. For IBD this is particularly relevant to the ever-expanding T<sub>H</sub> cell subsets and innate lymphoid cells which rely on staining cytoplasmic cytokines and/or nuclear transcription factors for their characterization (28). Definitively identifying these subsets

for *in vivo* imaging is difficult in live cells as antibodies are typically too large to passively enter cells.

In contrast, IL-1 $\beta$  has two favorable characteristics for immuno-PET. Firstly, it is inducible rather than constitutive and therefore is only secreted by activated cells which, in colitis, are predominately located at sites of inflammation. Secondly, proteolytic processing of IL-1 $\beta$  into its mature form typically occurs within the cell and it is secreted as a mature functional protein (29). This is somewhat of an anomaly for cytokines but is beneficial for immuno-PET as only mature IL-1 $\beta$  is imaged. Our results support further investigation into the use of imaging inducible and intracellularly processed immune mediators for detecting inflammation in IBD. Furthermore, immuno-PET using radiolabels with long half-lives, such as <sup>89</sup>Zr, enables longitudinal imaging which would provide valuable information regarding the temporal nature of immune responses in IBD.

SPECT is a cost-effective technique for nuclear imaging but generally has reduced resolution relative to PET. Nonetheless SPECT imaging of the neutrophil attracting chemokine CXCL8, and CD4 have also shown potential in pre-clinical and human studies of IBD (11, 12, 30). Furthermore, while SPECT imaging of the TNF- $\alpha$  neutralizing antibody infliximab also demonstrated some efficacy in pre-clinical colitis, it was hindered by high background which was likely due to its chimeric mouse/human properties (13). The most readily available alternative markers for immuno-PET imaging of IBD include antibodies that are currently used for treatment, including variations

targeting TNF- $\alpha$ ,  $\alpha_4\beta_7$  (vedolizumab),  $\alpha_4\beta_1$  (natalizumab) and IL-12/23 (Ustekinumab) (31). However, it should be noted that markers do not have to be limited to the immune system. Epithelial damage and increased epithelial barrier permeability are hallmark features of IBD and colitis, as we demonstrate in our model (32,33). The permeability of the epithelial monolayer to luminal contents is regulated by a large family of tight junction proteins, many of which are reduced in degraded tissue in the inflamed intestine impeding their use as markers. Conversely expression of some of these proteins promote increased permeability and are increased during IBD, such as the pore-forming Claudin-2 (34,35). Other potential markers include those associated with tissue remodeling associated with the resolution of inflammation (36). Matrix metalloproteases are involved in tissue remodeling and, interestingly, are thought to play a key role in promoting fibrosis. While an antibody against matrix metalloprotease 9 was ultimately withdrawn from clinical trials in IBD, interest in this target remains and it may have more promise as a marker of fibrosis (37).

The clinical utility of Immuno-PET for IBD is currently limited by several issues. Primarily, antibodies are large molecules with molecular weights of  $\sim 150$  kDa. This large size prolongs their half-life and reduces excretion, which is beneficial when used as treatments but is challenging for imaging as it reduces tissue penetration and prolongs excretion. Issues related to tissue penetration may be somewhat diminished in IBD as vascular permeability is increased in inflammation, aiding immune cell migration into inflammatory sites (38). However, increased leukocyte extravasation is unlikely to drastically reduce the time taken for systemically administered antibodies to reach

inflammatory sites in IBD, and the current clinical paradigm would require dosing and imaging to occur at separate visits over several days. This results in increased exposure to radiolabels, potentially increasing the risk of side effects. Promising alternatives to intact antibodies are in development that potentially limit these concerns (39). Notably, engineered small antibody fragments against anti-CD4 and  $\beta_7$  have already showed promise in pre-clinical colitis (9,10). A different strategy uses a 2-step process for pre-targeting; The initial step comprises of administration of an antibody modified to incorporate a radiolabel capture site, which is allowed enough time to localize to its target and a few days later the radiolabel is injected and binds to the antibody. This strategy has shown promise in cancer (40), but is yet to be applied to IBD and may prove to be difficult as the harsh protease rich environment in inflammation may rapidly degrade targets.

## **CONCLUSION**

In conclusion, we have demonstrated that radiolabeled antibodies against innate immune cells and mediators are suitable for immuno-PET of colitis. Our results provide further evidence warranting the clinical utility of immuno-PET for IBD diagnosis and monitoring. Development of these techniques would be of particular benefit to patients that are difficult to scope, including the pediatric population and those that have inflamed and/or fibrotic regions of the small intestine.

**Disclosure:** No authors have any personal or financial conflicts of interest

## **ACKNOWLEDGMENTS**

The authors acknowledge the facilities and scientific and technical assistance of the National Imaging Facility, a National Collaborative Research Infrastructure Strategy (NCRIS) capability, at the South Australian Health and Medical Research Institute (SAHMRI).

## REFERENCES

1. Abraham C, Cho JH. Inflammatory bowel disease. *N Engl J Med*. 2009;361:2066-2078.
2. Baumgart DC, Sandborn WJ. Inflammatory bowel disease: clinical aspects and established and evolving therapies. *Lancet*. 2007;369:1641-1657.
3. Sands BE. Biomarkers of Inflammation in Inflammatory Bowel Disease. *Gastroenterology*. 2015;149:1275-1285 e1272.
4. Caobelli F, Evangelista L, Quartuccio N, et al. Role of molecular imaging in the management of patients affected by inflammatory bowel disease: State-of-the-art. *World J Radiol*. 2016;8:829-845.
5. Allocca M, Fiorino G, Bonifacio C, et al. Comparative accuracy of bowel ultrasound versus magnetic resonance enterography in combination with colonoscopy in assessing Crohn's disease and guiding clinical decision-making. *J Crohns Colitis*. 2018.
6. Knowles SM, Wu AM. Advances in immuno-positron emission tomography: antibodies for molecular imaging in oncology. *J Clin Oncol*. 2012;30:3884-3892.
7. van Dongen GA, Visser GW, Lub-de Hooge MN, de Vries EG, Perk LR. Immuno-PET: a navigator in monoclonal antibody development and applications. *Oncologist*. 2007;12:1379-1389.
8. Bailly C, Clery PF, Faivre-Chauvet A, et al. Immuno-PET for Clinical Theranostic Approaches. *Int J Mol Sci*. 2016;18.
9. Freise AC, Zettlitz KA, Salazar FB, et al. Immuno-PET in Inflammatory Bowel Disease: Imaging CD4-Positive T Cells in a Murine Model of Colitis. *J Nucl Med*. 2018;59:980-985.
10. Dearling JL, Daka A, Veiga N, Peer D, Packard AB. Colitis ImmunoPET: Defining Target Cell Populations and Optimizing Pharmacokinetics. *Inflamm Bowel Dis*. 2016;22:529-538.
11. Gratz S, Rennen HJ, Boerman OC, Oyen WJ, Corstens FH. Rapid imaging of experimental colitis with (99m)Tc-interleukin-8 in rabbits. *J Nucl Med*. 2001;42:917-923.
12. Aarntzen EH, Hermsen R, Drenth JP, Boerman OC, Oyen WJ. 99mTc-CXCL8 SPECT to Monitor Disease Activity in Inflammatory Bowel Disease. *J Nucl Med*. 2016;57:398-403.
13. Tsoelas C, Penglis S, Ruskiewicz A, Bartholomeusz DL. Scintigraphic imaging of experimental colitis with technetium-99m-infliximab in the rat. *Hell J Nucl Med*. 2006;9:85-89.

14. Hofma BR, Wardill HR, Mavrangelos C, et al. Colonic migrating motor complexes are inhibited in acute tri-nitro benzene sulphonic acid colitis. *PLoS One*. 2018;13:e0199394.
15. Campaniello MA, Mavrangelos C, Eade S, et al. Acute colitis chronically alters immune infiltration mechanisms and sensory neuro-immune interactions. *Brain Behav Immun*. 2017;60:319-332.
16. Campaniello MA, Harrington AM, Martin CM, Ashley Blackshaw L, Brierley SM, Hughes PA. Activation of colo-rectal high-threshold afferent nerves by Interleukin-2 is tetrodotoxin-sensitive and upregulated in a mouse model of chronic visceral hypersensitivity. *Neurogastroenterol Motil*. 2016;28:54-63.
17. Holland JP, Sheh Y, Lewis JS. Standardized methods for the production of high specific-activity zirconium-89. *Nucl Med Biol*. 2009;36:729-739.
18. Vosjan MJ, Perk LR, Visser GW, et al. Conjugation and radiolabeling of monoclonal antibodies with zirconium-89 for PET imaging using the bifunctional chelate p-isothiocyanatobenzyl-desferrioxamine. *Nat Protoc*. 2010;5:739-743.
19. Holland JP, Divilov V, Bander NH, Smith-Jones PM, Larson SM, Lewis JS. 89Zr-DFO-J591 for immunoPET of prostate-specific membrane antigen expression in vivo. *J Nucl Med*. 2010;51:1293-1300.
20. Yushkevich PA, Piven J, Hazlett HC, et al. User-guided 3D active contour segmentation of anatomical structures: significantly improved efficiency and reliability. *Neuroimage*. 2006;31:1116-1128.
21. Neurath MF. Cytokines in inflammatory bowel disease. *Nat Rev Immunol*. 2014;14:329-342.
22. Kiesler P, Fuss IJ, Strober W. Experimental Models of Inflammatory Bowel Diseases. *Cell Mol Gastroenterol Hepatol*. 2015;1:154-170.
23. Rivera-Nieves J. Strategies that target leukocyte traffic in inflammatory bowel diseases: recent developments. *Curr Opin Gastroenterol*. 2015;31:441-448.
24. Mowat AM, Agace WW. Regional specialization within the intestinal immune system. *Nat Rev Immunol*. 2014;14:667-685.
25. Ehirchiou D, Xiong Y, Xu G, Chen W, Shi Y, Zhang L. CD11b facilitates the development of peripheral tolerance by suppressing Th17 differentiation. *J Exp Med*. 2007;204:1519-1524.

- 26.** Shen S, Prame Kumar K, Stanley D, et al. Invariant Natural Killer T Cells Shape the Gut Microbiota and Regulate Neutrophil Recruitment and Function During Intestinal Inflammation. *Front Immunol.* 2018;9:999.
- 27.** Zola H, Swart B, Nicholson I, Voss E. Leukocyte and stomal cell markers : The CD markers. Hoboken, New Jersey, USA: John Wiley and Sons, Inc. ; 2006:58-59.
- 28.** Goldberg R, Prescott N, Lord GM, MacDonald TT, Powell N. The unusual suspects--innate lymphoid cells as novel therapeutic targets in IBD. *Nat Rev Gastroenterol Hepatol.* 2015;12:271-283.
- 29.** Afonina IS, Muller C, Martin SJ, Beyaert R. Proteolytic Processing of Interleukin-1 Family Cytokines: Variations on a Common Theme. *Immunity.* 2015;42:991-1004.
- 30.** Kanwar B, Gao DW, Hwang AB, et al. In vivo imaging of mucosal CD4+ T cells using single photon emission computed tomography in a murine model of colitis. *J Immunol Methods.* 2008;329:21-30.
- 31.** Danese S, Vuitton L, Peyrin-Biroulet L. Biologic agents for IBD: practical insights. *Nat Rev Gastroenterol Hepatol.* 2015;12:537-545.
- 32.** Ahmad R, Sorrell MF, Batra SK, Dhawan P, Singh AB. Gut permeability and mucosal inflammation: bad, good or context dependent. *Mucosal Immunol.* 2017;10:307-317.
- 33.** McGuckin MA, Eri R, Simms LA, Florin TH, Radford-Smith G. Intestinal barrier dysfunction in inflammatory bowel diseases. *Inflamm Bowel Dis.* 2009;15:100-113.
- 34.** Landy J, Ronde E, English N, et al. Tight junctions in inflammatory bowel diseases and inflammatory bowel disease associated colorectal cancer. *World J Gastroenterol.* 2016;22:3117-3126.
- 35.** Luissint AC, Parkos CA, Nusrat A. Inflammation and the Intestinal Barrier: Leukocyte-Epithelial Cell Interactions, Cell Junction Remodeling, and Mucosal Repair. *Gastroenterology.* 2016;151:616-632.
- 36.** Lawrance IC, Rogler G, Bamias G, et al. Cellular and Molecular Mediators of Intestinal Fibrosis. *J Crohns Colitis.* 2017;11:1491-1503.
- 37.** Neurath M. Current and emerging therapeutic targets for IBD. *Nat Rev Gastroenterol Hepatol.* 2017;14:688.
- 38.** Rampton DS, Collins CE. Review article: thromboxanes in inflammatory bowel disease--pathogenic and therapeutic implications. *Aliment Pharmacol Ther.* 1993;7:357-367.

39. Freise AC, Wu AM. In vivo imaging with antibodies and engineered fragments. *Mol Immunol.* 2015;67:142-152.
40. Foubert F, Gouard S, Sai-Maurel C, et al. Sensitivity of pretargeted immunoPET using (68)Ga-peptide to detect colonic carcinoma liver metastases in a murine xenograft model: Comparison with (18)FDG PET-CT. *Oncotarget.* 2018;9:27502-27513.

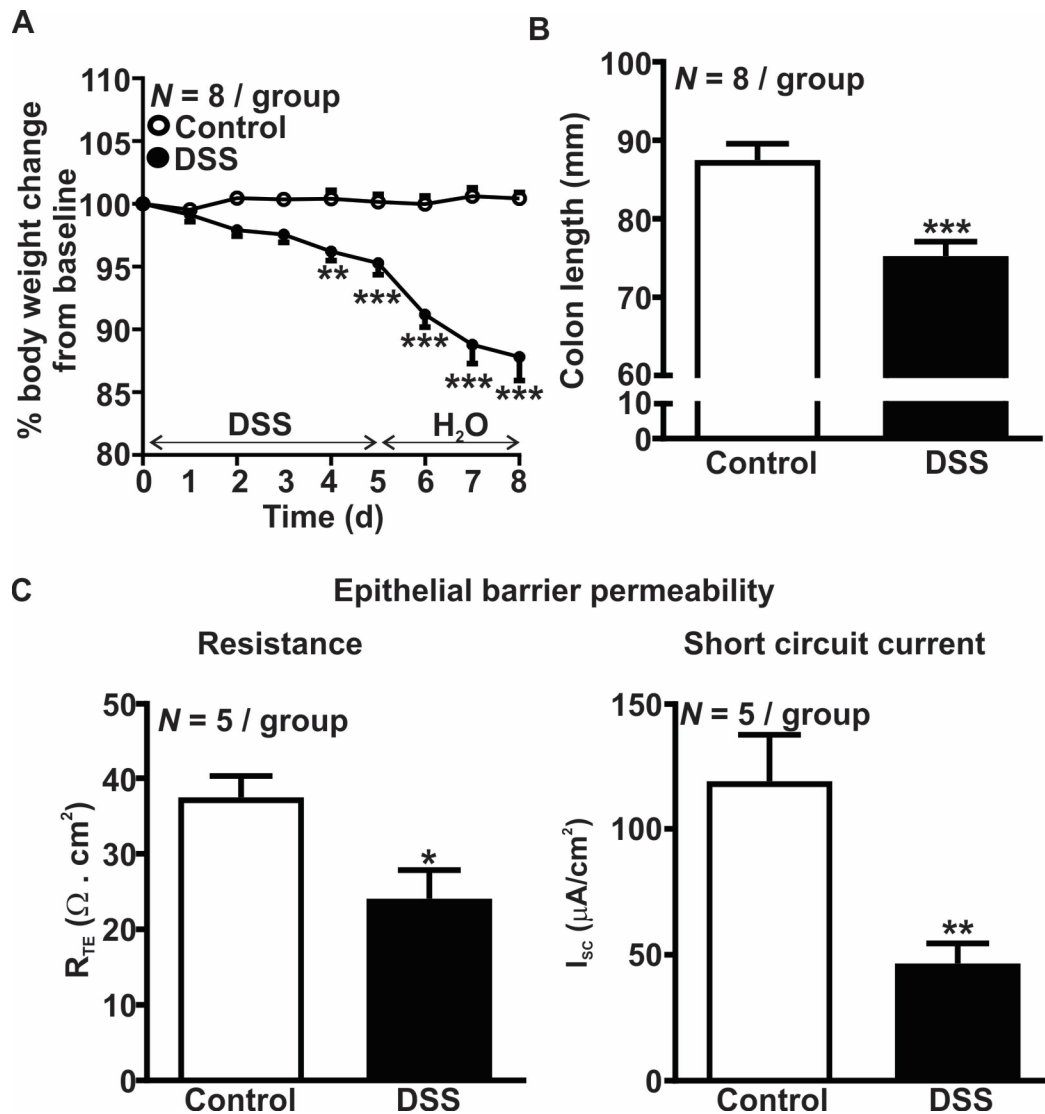


**Figure 1.** Characterization of DSS colitis. (A) DSS colitis caused a loss of body weight, (B) shortening of colon length and (C) impaired epithelial barrier trans-epithelial electric resistance (left) and short-circuit current (right). \**P* < 0.05, \*\**P* < 0.01, \*\*\* *P* < 0.001.

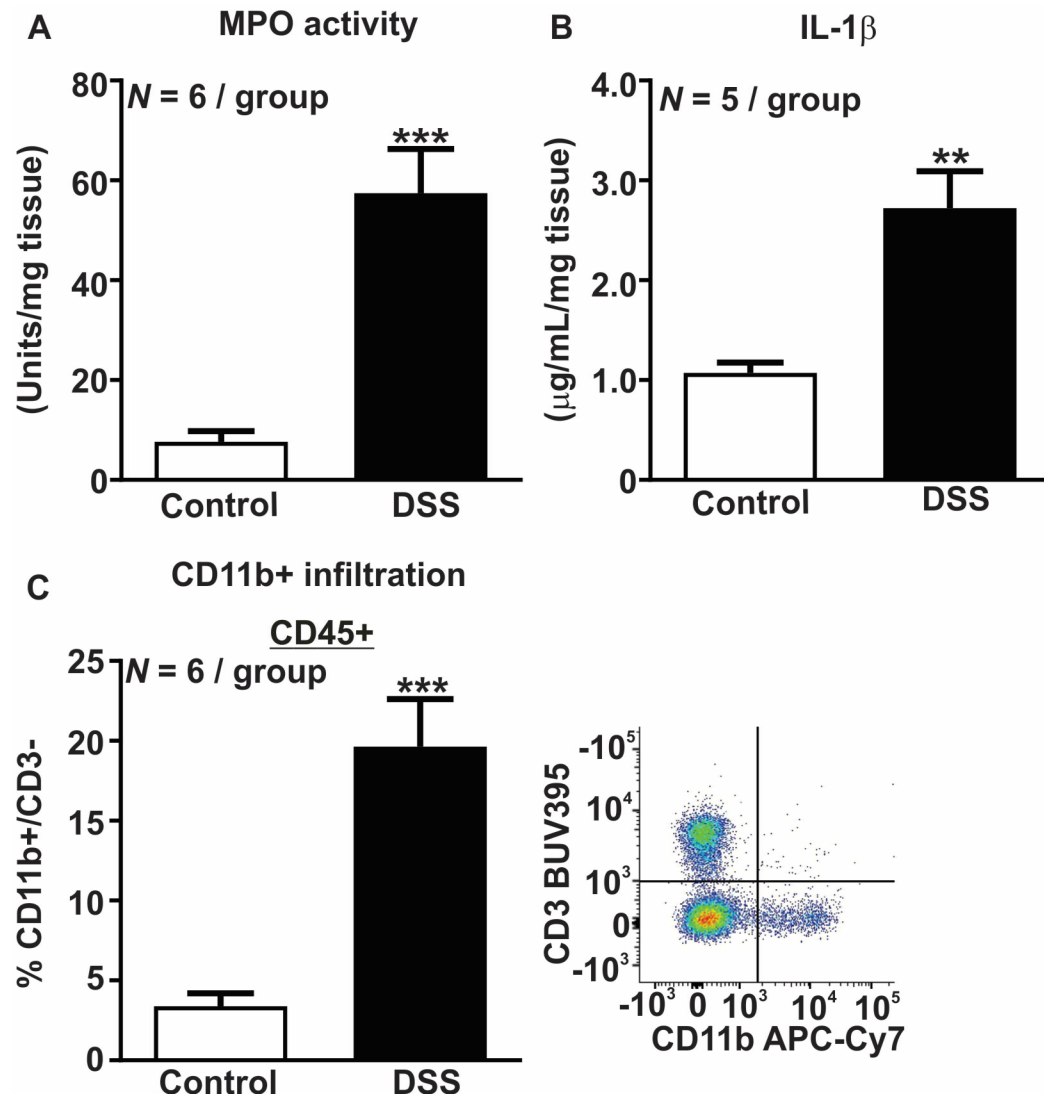


**Figure 2.** DSS colitis activated the innate immune system. (A) Colonic MPO activity, (B) IL-1 $\beta$  concentrations and (C) CD11b+ CD3- innate immune cell infiltration were increased in DSS colitic mice. Image represents gating strategy. \*\*P < 0.01, \*\*\* P < 0.001.

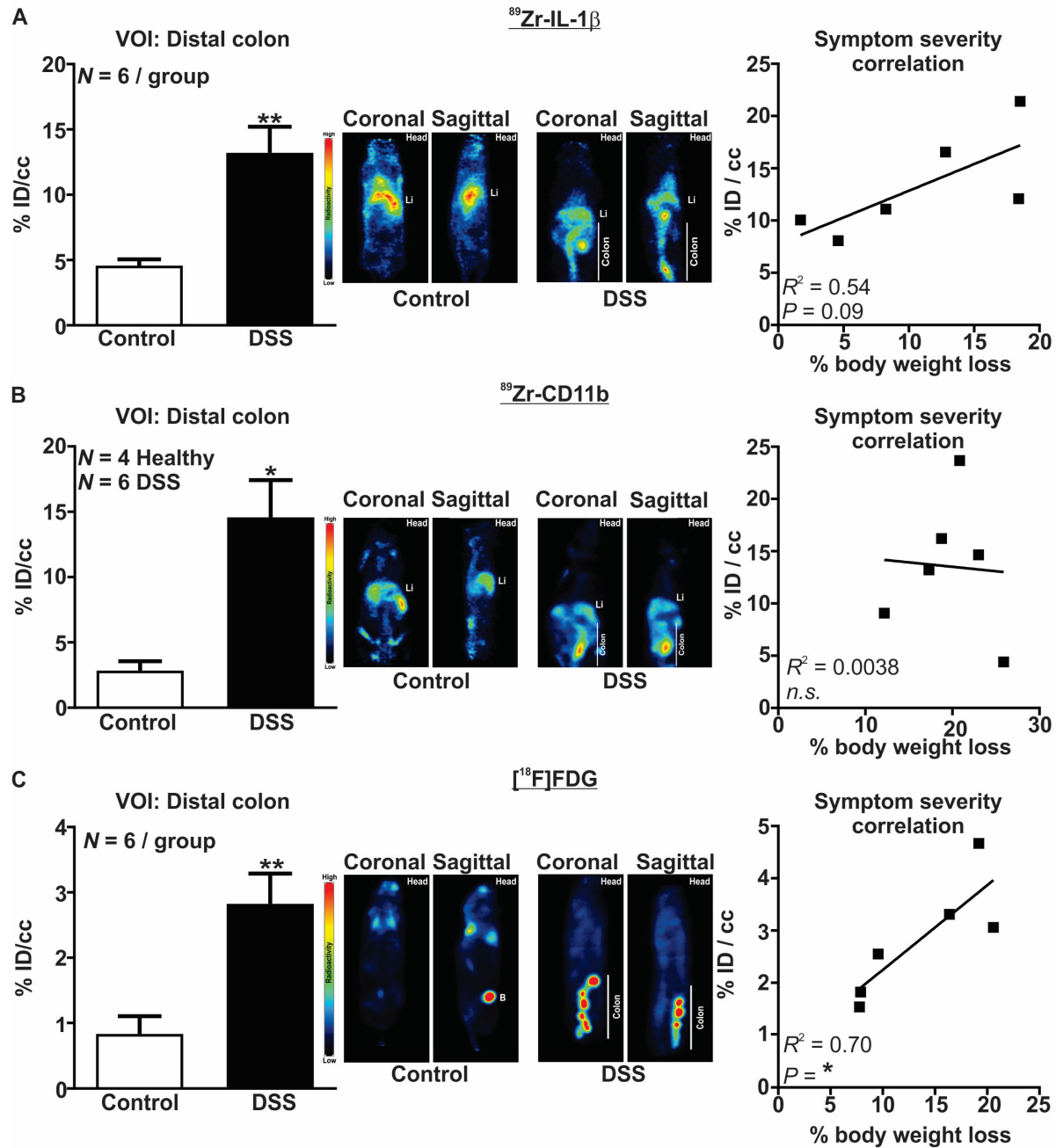


**Figure 3.**  $\alpha$ -IL-1 $\beta$ ,  $\alpha$ -CD11b and  $^{18}\text{F-FDG}$  PET detection of colonic inflammation. Volume of interest (VOI) analysis with representative PET image (coronal and sagittal) of control and DSS mice (left) and correlation of % body weight loss with VOI (right) for (A)  $^{89}\text{Zr-}\alpha$ -1L-1 $\beta$ , (B)  $^{89}\text{Zr-}\alpha$ -CD11b and (C)  $^{18}\text{F-FDG}$ . Li = Liver, B= bladder. \* $P < 0.05$ , \*\* $P < 0.01$ .

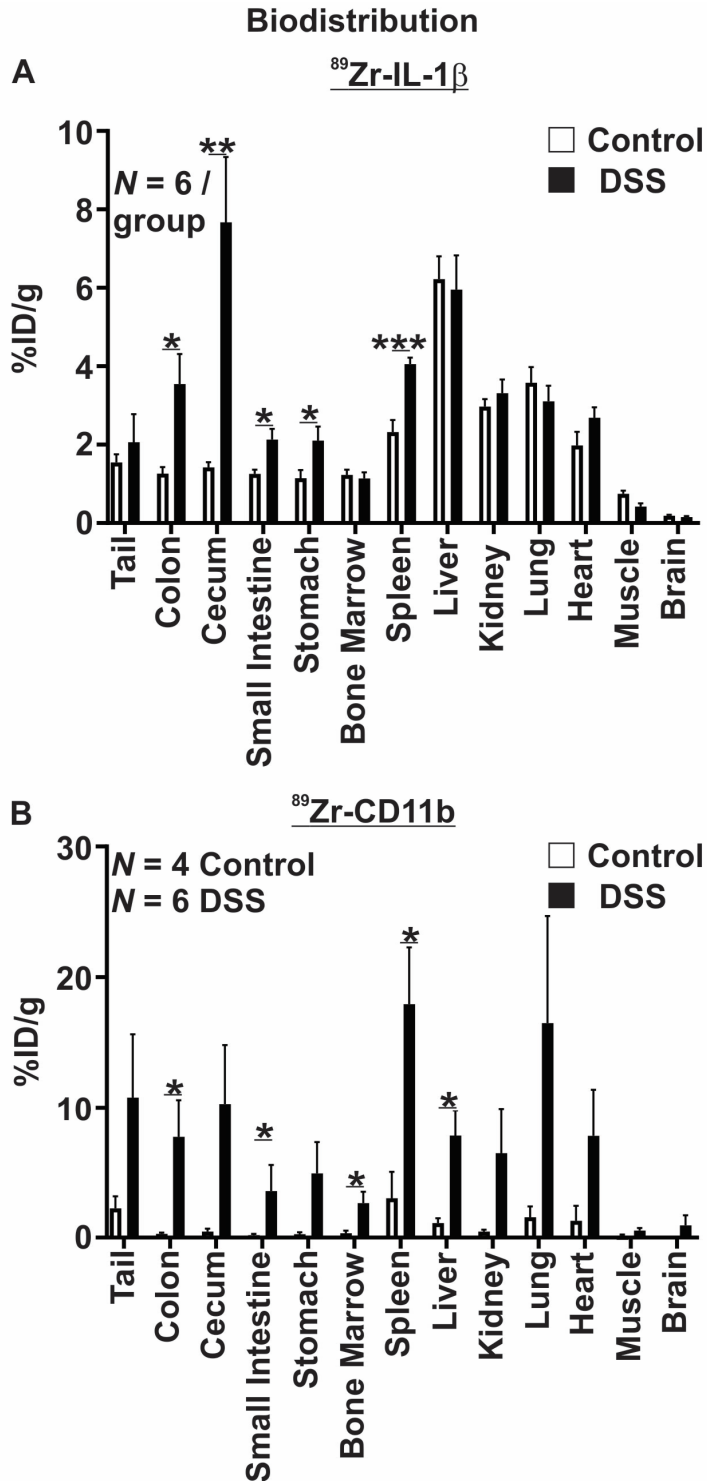


**Figure 4.** Ex vivo biodistribution of (A)  $^{89}\text{Zr-}\alpha\text{-1L-1}\beta$  and (B)  $^{89}\text{Zr-}\alpha\text{-CD11b}$ . Decay-corrected values for uptake are displayed. \* $P < 0.05$ , \*\* $P < 0.01$ , \*\*\* $P < 0.001$ .

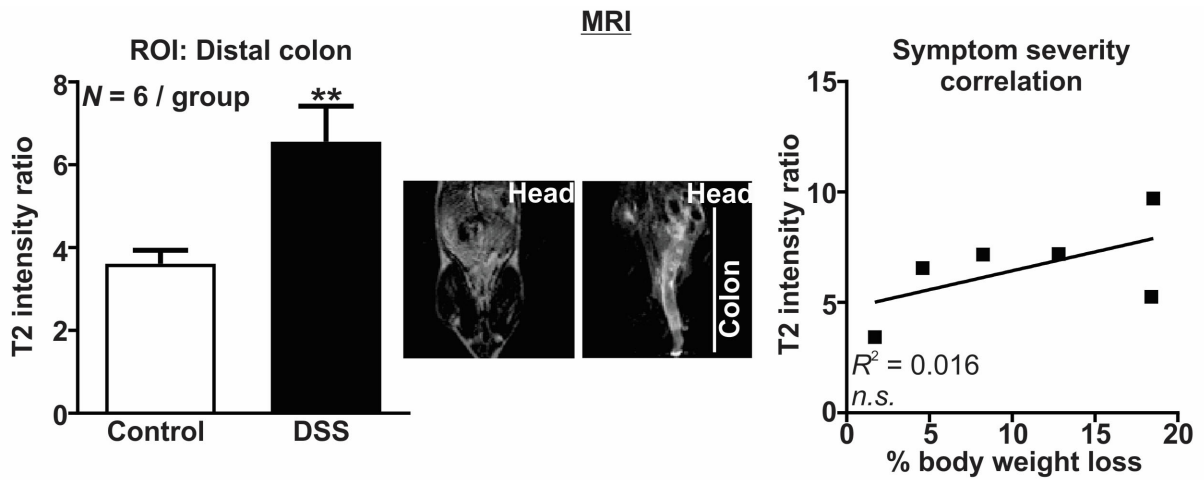


**Figure 5.** MRI detection of colonic inflammation. Region of interest (ROI) analysis with representative MRI image (coronal) of control and DSS mice (left) and correlation of % body weight loss with ROI MRI analysis (right). \*\**P* < 0.01.